09,16

Electron beam-induced color and phosphorescence centers in transparent ceramics based on yttria with additives of zirconium and ytterbium

© V.I. Solomonov, A.S. Makarova, A.V. Spirina, V.V. Osipov, A.N. Orlov, V.A. Shitov

Institute of Electrophysics, Ural Branch of the Russian Academy of Sciences, Yekaterinburg, Russia

E-mail: plasma@iep.uran.ru

Received June 5, 2025
Revised June 5, 2025
Accepted June 26, 2025

After irradiation with nanosecond (2 ns) electron beams with an average energy of 170 keV, initially colorless transparent ceramic samples of $Y_2O_3 + 5$ mol.% ZrO_2 and $Yb:Y_2O_3 + 5$ mol.% ZrO_2 compositions are colored. At the same time, transmittance spectra of the ceramics show an absorption band at 487 nm, which, along with the color intensity, increases with increasing number of irradiation pulses. After being irradiated, the ceramic color spontaneously restores with a time constant of about 80 h at room temperature. It is shown that the coloring of ceramics is caused by F-type centers. In addition, the $Yb:Y_2O_3 + 5$ mol.% ZrO_2 samples exhibit phosphorescence in a broad band of 890–1200 nm, the intensity of which decreases according to a hyperbolic law with a characteristic time of about 10 s. A model for the mechanisms of coloration and discoloration of the ceramics is proposed.

Keywords: light transmittance kinetics, nanopowder, transmittance spectrum, luminescence decay.

DOI: 10.61011/PSS.2025.06.61696.107-25

1. Introduction

Ceramics based on ytterbium-activated yttria ($Yb:Y_2O_3$) is a promising material for active elements of powerful lasers [1–3]. The Yb^{3+} activator ion has a simple energy structure consisting of two levels: upper $^2F_{5/2}$ and lower $^2F_{7/2}$, split in a crystalline field into three and four Stark components, respectively. Laser generation at wavelengths of 1030 and 1074 nm is excited in optical transitions from the lowest $^2F_{5/2}$ Stark sublevel to the upper $^2F_{7/2}$ Stark sublevels. The ceramic technology of manufacturing of the active laser elements based on $Yb:Y_2O_3$ uses sintering additives, in particular, in the form of heterovalent zirconium ions [4]. Under the external high energy exposure, for example, when irradiated with electrons, such ceramics may experience spatial displacement or charge variation of impurity ions and their environment. This may cause formation of new induced defective structures, including color and absorption centers. In particular, in [5] the darkening of ytterbia-doped aluminosilicate light diodes is attributed to the presence of Yb^{2+} ion.

The purpose of the paper is to study the kinetics of light transmission (transparency) and luminescence of ceramics based on Y_2O_3 with addition of Yb_2O_3 and ZrO_2 oxides depending on the number of irradiation pulses of ceramics with electron beams with an average energy of 170 keV and an energy density in the beam of 44.2 mJ/cm^2.

2. Samples and research methods

Samples of transparent yttria-based ceramics of three compositions were studied: $Yb_{0.1}Y_{1.9}O_3$ is the first group, $Y_2O_3 + 5$ mol.% ZrO_2 is the second group and $Yb_{0.1}Y_{1.9}O_3 + 5$ mol.% ZrO_2 is the third group. Nanopowders of the corresponding chemical composition were used to synthesize the ceramics.

Nanopowders were prepared by method of evaporation of a solid porous target by radiation of a fiber ytterbium laser [6]. The target was prepared from a mix of commercial grade microsize powders of yttrium, ytterbium, and zirconium oxides with purity of 99.99, 99.6, and 99.5%. Ytterbium oxide with a content of 5 mol.% was used as a laser active impurity. Zirconium oxide of the same content in the samples of the second and third group was used as a sintering additive. After condensation of vapors in the air the powder was formed, the primary content (98–99 %) of which were nanoparticles of the corresponding chemical composition with the average size of around 15 nm. The rest of the content (1–2 %) were particles of micron and submicron size.

Phase composition of powders was measured using diffractometer D8 Discover with a graphite monochromator on a diffracted beam ($\lambda = 0.1542$ nm — $K_{\alpha 1,2}$ copper). It is shown that the particles were crystallized in a monoclinic phase. After annealing in air at 900–1100 °C for 3 h, the particles transitioned to the cubic phase. This mode of phase transformation was accompanied by minor agglomeration of nanoparticles, which was confirmed by reduction of

Conditions for temperature treatment of process stages of nanopowders required to synthesize optic ceramics

Group	Chemical composition	Annealing of compact in air	Vacuum sintering	HIP in argon	Bleaching annealing of ceramics in air
1	$Yb_{0.1}Y_{1.9}O_3$	800 °C 3 h	1400 °C 1 h	1500 °C 2 h	1200 °C 10 h
2	$Y_2O_3 + 5$ mol.% ZrO_2	800 °C 3 h	1780 °C 20 h	–	1400 °C 2 h
3	$Yb_{0.1}Y_{1.9}O_3 + 5$ mol.% ZrO_2	900 °C 3 h	1750 °C 5 h	–	1400 °C 2 h

the specific surface area of nanoparticles measured by Brunauer–Emmett–Teller method. No second phases were found in nanopowders within the measurement error margin.

The produced nanopowders without addition of any organic binders were compacted with uniaxial static pressing under a pressure of 200 MPa into discs with a diameter of ~ 15 mm and a thickness of 3–4 mm with a density of around 45% relative to the theoretical density of crystal. The produced compacts were annealed in an atmospheric furnace to remove mechanical stresses and organic compounds. The first group ceramic samples were synthesized using method of hot isostatic pressing (HIP) at AIP HIP 6-30H setup (American Isostatic pressing, USA) under a pressure of 200 MPa with pre-sintering in a vacuum furnace. Synthesis of ceramics of the second and third groups was conducted in a vacuum furnace with tungsten heaters at a residual pressure $1 \cdot 10^{-3}$ Pa. High vacuum was pulled by using an assembly of a spiral (ANEST IWATA, Japan) and a turbomolecular (Shimadzu, Japan) pumps. Then all samples were exposed to bleaching annealing in air. The table presents the conditions of temperature treatment for process stages of nanopowder in each group.

X-ray diffraction analysis showed that the crystalline structure of ceramics was a solid solution of impurity elements (Yb, Zr) in the cubic lattice of yttrium oxide.

The ceramic samples were irradiated in the CLAVI setup [7] in air at room temperature with 2 ns-duration pulsed electron beams with an average electron energy of 170 keV, an electron current density of 130 A/cm^2 and an energy density per pulse of 44.2 mJ/cm^2. Irradiation pulse frequency was 1 Hz.

Transmittance spectra before and after irradiation of ceramic samples were measured in the range from 200 to 1100 nm using Shimatzu UV-1700 spectrophotometer.

To record the phosphorescence of the samples after their irradiation with electron beams, the emission from the sample surface was transmitted via a quartz light guide through a mechanical modulator to a photomultiplier tube (PMT) photocathode. With the purpose to determine the spectral range of the phosphorescence band, FEU-62 (operating range 400–1200 nm) or FEU-100 (200–800 nm) were used, as well as light filters. Signals from PMTs were recorded by means of a microprocessor control unit of MDR-41 monochromator with the use of MdrWin software.

Kinetics of Yb^{3+} emission band at 1030 nm was recorded by a FEU-62 photomultiplier tube and KeySight DSOX 2014A oscilloscope (100 MHz) under irradiation with single electron beam pulses. The band was selected by a MDR-41 monochromator with an inlet filter 1.0–1.5 μm and a diffraction grating 1200 grooves/mm at an entrance slit width of 2 mm (width of the recorded spectrum region was 5 nm).

3. Study results

Prior to irradiation with a pulsed electron beam all ceramic samples were colorless and transparent. After irradiation the first group ceramic samples ($Yb_{0.1}Y_{1.9}O_3$) remained colorless, while the third group ceramic samples ($Yb_{0.1}Y_{1.9}O_3 + 5$ mol.% ZrO_2) became orange-pink (Figure 1). Their coloring is also observed when irradiated with a mercury bactericide lamp ($\lambda = 254$ nm). After electron beam irradiation the second group ceramic samples $Y_2O_3 + 5$ mol.% ZrO_2 were also colored, but with less color intensity. Due to low color rendering of the camera, it was not possible to obtain a picture of these ceramics with a clear boundary of the irradiated and non-irradiated halves of the samples, therefore it is not provided.

Transmittance spectra of the ceramic samples of all three groups before and after irradiation with electron beams are provided in Figure 2. In the samples of the first group the transmittance spectra before and after irradiation does not

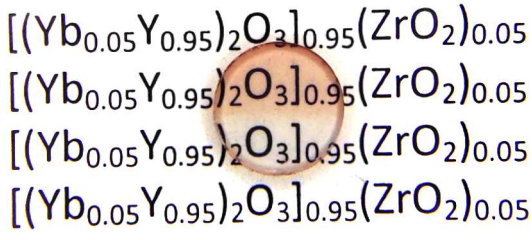

Figure 1. Picture of a ceramic $Yb_{0.1}Y_{1.9}O_3 + 5$ mol.% ZrO_2 sample, half of which has been irradiated with 500 electron beam pulses (upper), and the second half has been shielded with a lead plate (lower).

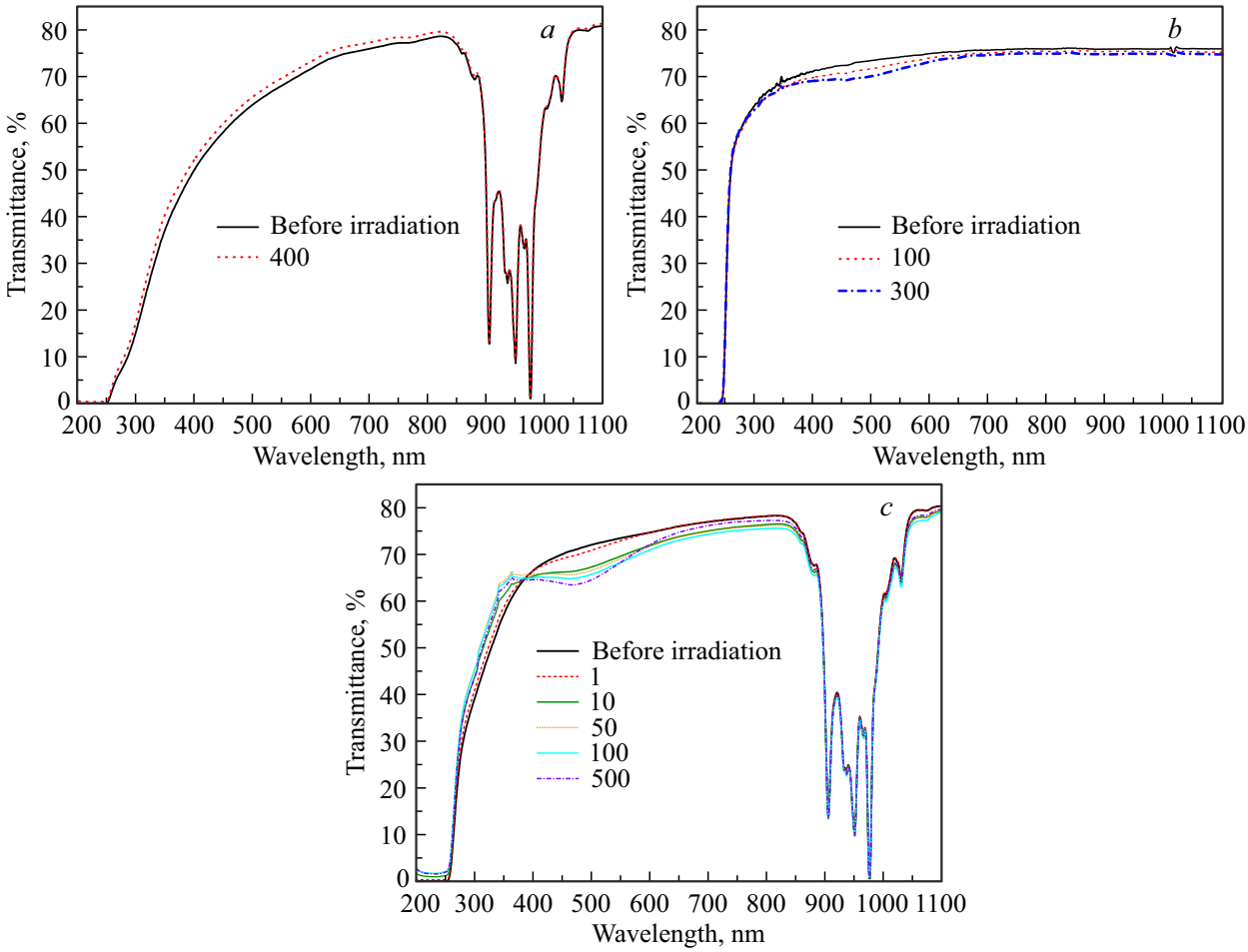

Figure 2. Transmittance spectra of ceramic samples in the *a*) first, *b*) second and *c*) third groups before and after irradiation with different number (specified in the Figure) of electron beam pulses.

change from a quality point of view (Figure 2, *a*). In the transmittance spectra of the first and third group samples the strong absorption lines of the Yb^{3+} ion are observed (Figure 2, *a* and *c*). After irradiation in the transmittance spectra of the second and third group samples, there is an additional wide absorption band with the maximum at 487 nm (Figure 2, *b* and *c*), which is stronger in the third group samples (Figure 2, *c*). As the number of irradiation pulses increases from 1 to 500 for samples of the third group, the absorption (optical density) in this band increases (Figure 3, *a*), and after sample irradiation it decays accordingly nearly to an exponential law with the characteristic decoloration time of $\tau_{dc} \approx 80$ h (Figure 3, *b*).

In the area 200–400 nm the increase in the light transmission of the third group samples irradiated with electron beams (Figure 2, *c*) was observed, and the difference in the transmittance of the irradiated and non-irradiated sample gradually reduced within 20 min after the external exposure stopped. Upon expiration of this time the transmittance spectrum in the UV region started corresponding to the spectrum of the sample not exposed to irradiation (Figure 2, *c*, black curve). Bleaching is false, and it happens as a result of instrumental distortions associated with the fact that irradiated samples exhibit phosphorescence in the spectrum region invisible to the eye. No glow of the samples was recorded in the spectral range of FEU-100 sensitivity, whereas FEU-62 consistently recorded their long-term afterglow (Figure 4, *a*). We were unable to confirm the structure of this band using a monochromator due to low spectral radiation density. However, the use of light filters made it possible to narrow the spectral range of the phosphorescence band to 890–1200 nm region. Its decay (Figure 4, *b*) with the correlation coefficient $R_2 = 0.99$ is described by a sum of two exponentials of type

$$I_p = A \exp\left(-\frac{t}{\tau_1}\right) + B \exp\left(-\frac{t}{\tau_2}\right) \quad (1)$$

with characteristic times $\tau_1 \approx 10.4$ s and $\tau_2 \approx 145$ s (Figure 4, *b*, red dotted straight lines), and by hyberbolic law

$$I(t) = I_0 \left(1 + \frac{t}{\tau}\right)^{-2} \quad (2)$$

with $\tau \approx 10$ s (Figure 4, *b*, green dotted straight line), where $I(t)$ and I_0 are current and initial intensity of phosphorescence.

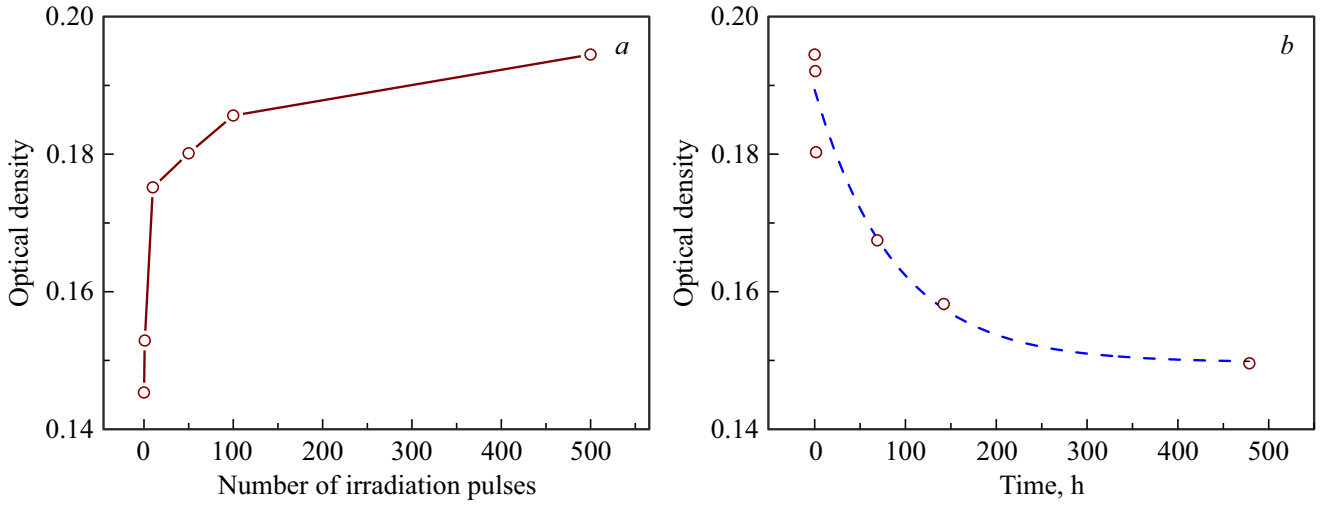

Figure 3. Change in optical density in the absorption band at 487 nm in the third group samples with the increase in the number of electron beam irradiation pulses (*a*) and in time after irradiation with 500 pulses (*b*). Blue dotted curve is the result of approximation with the exponential function.

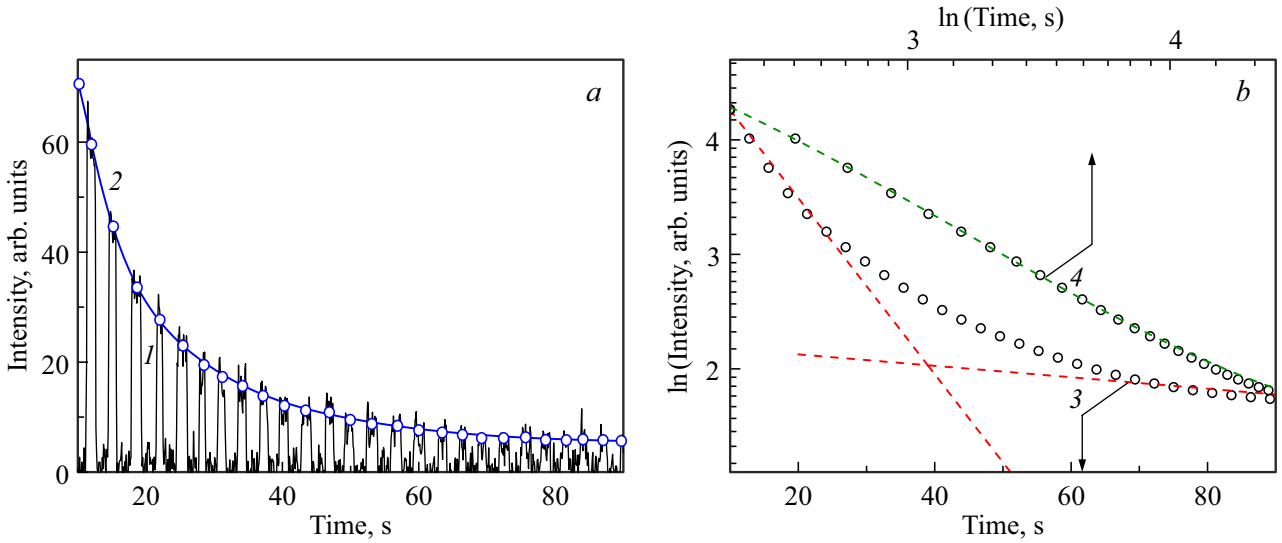

Figure 4. Phosphorescence kinetics of the third group ceramic sample after irradiation with electrons: *a*) signal from FEU-62: curve *1* — initial modulated phosphorescence signal, *2* — envelope curve along the maxima; *b*) estimation of characteristic decay time: *3* — curve *2* in logarithmic coordinates along intensity axis, red dotted straight lines show approximation with function (*1*), *4* — curve *2* in logarithmic coordinates along the intensity and time axes, dotted green straight line is the result of approximation by function (*2*).

For the third group samples, the decay kinetics of pulsed cathodoluminscescence was recorded in the band at 1030 nm, corresponding to the laser transition of Yb^{3+} ion. Luminescence decay curves were recorded for every previously non-irradiated sample after 1st, 10th, 20th, 30th, . . . , 200th irradiation pulse. The time between measurements was around 1 min. Photocurrent (I_p) decay curves for all samples were similar (Figure 5).

All decay curves I_p of the third group samples after the first irradiation pulse are fitted with the correlation coefficient $R_2 > 0.96$ by the sum of two exponents (1) with characteristic times $\tau_1 = 70.2 \pm 5.1\,\mu$s and $\tau_2 = 1.64 \pm 0.08$ ms. (Here the error is the spread of these values over 9 measurements — number of the third group samples). As the number of irradiation pulses increases to $N \approx 60$, the long-term component τ_2 has a trend towards decrease from 1.64 to 1.48 ms, but at $N \geq 60$ both characteristic times maintain their values within $\tau_1 = 70.0 \pm 4.4\,\mu$s and $\tau_2 = 1.51 \pm 0.07$ ms. Ratio of coefficients A/B increases with the increase of N up to 60, and at $N \geq 60$ it maintains its value of 6.2 ± 0.4.

When the same ceramic samples are photoexcited by a laser diode having an operating wavelength of 976 nm, the kinetics of this band is described well by one exponential function with the characteristic time close to τ_2.

4. Discussion of results

In all ceramic samples prior to electron beam irradiation the optically active centers do not manifest themselves (Figure 2). Exposure to the electron beam stimulates rearrangement of defects and their optical activation in the ceramics of the second and third groups (with zirconium oxide as a sintering additive). Therefore, the absorption band at 487 nm appearing in this ceramics after electron beam irradiation is indirectly related to the presence of quadrivalent Zr^{4+} ions therein. The Zr^{4+} ion itself, having a closed electron shell, is optically inactive in the visible region of the spectrum. Trivalent ions of zirconium that may be present or be created in the ceramics with beam electrons must manifest themselves in absorption at $d \rightarrow d$- ($E \rightarrow T_2$) transitions in the longer wavelength range of 590–620 nm. In luminescence the trivalent ions of zirconium in yttria-based ceramics manifest themselves in the bands at $\lambda \approx 818$ and 900 nm [8].

Spectral position and kinetics of the wide absorption band at 487 nm comply well with the F-type center. In aluminum oxide such absorption band at 490 nm is attributed to F_2^{2+}-center [9]. Such centers may appear in the Y_2O_3 crystalline lattice of the cubic phase, containing zirconium. Therein the Zr^{4+} ions substitute the main Y^{3+} cations, which are located in the center of an elemental cube YO_6. Besides, in 3/4 of these cubes the natural oxygen vacancies are located at the vertices along the face diagonal line, and in 1/4 of the cubes they are located along the space diagonal line [10]. As the zirconium ions in the quadrivalent state enter, to compensate for their electric charge, the elemental cubes may be built to ZrO_8 by displacement of the oxygen ions from the adjacent elemental cubes. As a result some of these adjacent cubes change into distorted polyhedra with oxygen vacancies (V_O). Besides, the yttria ceramics includes oxygen vacancies formed because of oxygen evaporation during high temperature vacuum sintering of ceramics. The subsequent bleaching annealing in air does not fully compensate for oxygen deficiency. Therefore, the absorption band at 487 nm, present in the ceramic samples from yttrium oxide with addition of zirconium oxide as a sintering additive, must be attributed to the absorption of F-type center. Besides, this center is formed in process of electron beam action as free electrons are captured by oxygen vacancies. The F-type color centers that are produced during this process are rather long-lived. In the first 478 h after electron beam irradiation, the decrease in optical density in the absorption band follows an exponential law with a characteristic time of around 80 h.

Only the third group ceramic samples exhibit phosphorescence in the region of 890–1200 nm after their electron beam irradiation. This makes it possible to assume that ytterbium and zirconium ions participate in generation of the centers responsible for this emission band. The hyperbolic nature of decay of this phosphorescence band makes it possible to assume that it is the result of the radiative recombination of electron and hole centers.

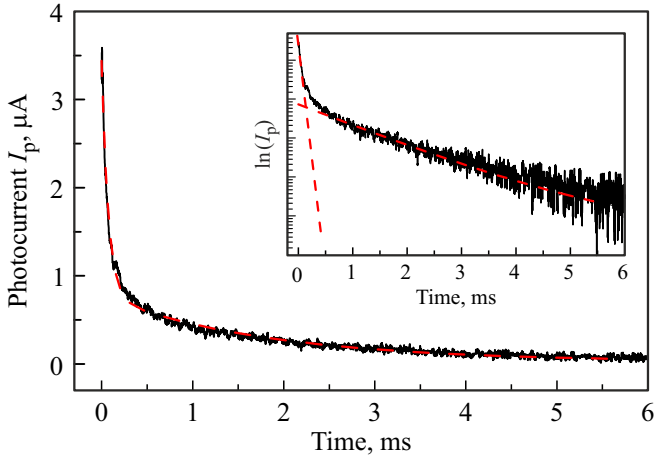

Figure 5. Decay of photocurrent I_p from luminescence signal at a wavelength of 1030 nm in a third group sample. Dotted red line is the result of approximation with function (1). The insert shows a decay curve in logarithmic scale along I_p axis.

These centers may be Yb^{2+} and O^{1-} ions formed as a result of charge transfer during the electron beam action in Zr^{4+} ion-distorted polyhedra. Previously [4] when the Raman scattering spectra of laser radiation at a wavelength of 785 nm were studied, the wide photoluminescence band 890–1050 nm was found in the third group samples. In [4] this band has been shown to be of complicated composition. It includes IR-bands of Yb^{3+} ion emission. Photoexcitation at a wavelength of 785 nm indicates that these centers may be present in the samples that were not previously electron beam irradiated. In particular, they may represent Yb^{2+} ions located in the distorted polyhedra or stabilized with organic radicals that are present in the samples in small quantities.

Currently the spectral position of the energy levels of Yb^{2+} ion in the yttrium oxide has not been experimentally found. Based on the reference data for a free Yb^{2+} ion and Stark splitting in the crystalline field of cubic symmetry [11,12], $4f^{13}5d^1$ configuration levels of this ion are arranged $(30-55)\cdot 10^3\,cm^{-1}$ higher than the ground $4f^{14}(^1S_0$ state). At the width of the band gap in yttrium oxide at around $40000\,cm^{-1}$ (250 nm, the boundary of fundamental absorption in Figure 2) the upper energy band of the $4f^{13}5d^1(^2F_{5/2}t_{2g})$ orbital triplet is located in the conduction band, whereas the lower band of the $4f^{13}5d^1(^2F_{7/2}t_{2g})$ triplet and two bands of the $4f^{13}5d^1(^2F_{7/2,5/2}e_g)$ orbital doublet, same as in the yttrium-aluminum garnet [11], may be located in the band gap. Transitions from the ground state of the Yb^{2+} ion to these levels must appear as absorption bands in the visible and ultraviolet regions of the spectrum. However, in the transmittance spectra (Figure 2) of ytterbium-containing ceramics, there are no absorption bands that may be associated with these transitions.

At the same time the energy position of Yb^{2+} ion levels in the Zr^{4+} ion-distorted polyhedra may be substantially different. Namely, levels of bands of the $4f^{13}5d^1(^2F_{7/2,5/2}e_g)$

orbital doublet may have a lower position sufficient for their excitation with radiation having a wavelength of 785 nm [4]. Besides, when samples are electron beam irradiated, Yb^{2+} ions may be additionally generated in the process of electron capture by excited $Yb^{3+}(^2F_{5/2})$ ion with a characteristic time of 70 μs. This process is reflected in the decay kinetics of pulsed cathodoluminscescence at 1030 nm band (Figure 5). It clearly shows two exponential mechanisms of intensity decrease with characteristic times: $\tau_1 = 70.2 \pm 5.1\,\mu$s and $\tau_2 = 1.64 \pm 0.08$ ms, whereas when photoexcitated with a laser diode having an operating wavelength of 976 nm, the same ceramic samples lack the fast component τ_1 in the kinetics of this band. Therefore, it should be deemed that the characteristic time $\tau_2 = 1.64 \pm 0.08$ ms is the lifetime of $^2F_{5/2}$ level for Yb^{3+} ion, and $\tau_1 \approx 70.2 \pm 5.1\,\mu$s reflects the de-excitation rate of the $^2F_{5/2}$ radiative level by electron capture. Therefore, the contribution of additional de-excitation mechanism to the integral intensity of the Yb^{3+} ion band at 1030 nm can be estimated as

$$(A \cdot \tau_1)/(B \cdot \tau_2) \approx 0.15{-}0.28. \qquad (3)$$

Here A and B are the coefficients of approximating expression (1). In the first approximation, the expression (3) provides the estimate of the ratio between contents of di- and trivalent ytterbium ions in the samples.

5. Conclusion

The conducted studies found that color centers of F-type appear in the ceramic samples based on yttrium oxide containing zirconium oxide ($Y_2O_3 + 5$ mol.% ZrO_2 and $Yb:Y_2O_3 + 5$ mol.% ZrO_2) after irradiation by nanosecond electron beams with an average energy of 170 keV and a current density of 130 A/cm^2. Their spontaneous decay at room temperature occurs at an exponential rate with the characteristic time of around 80 h.

In the ceramic samples containing zirconium and ytterbium ($Yb:Y_2O_3 + 5$ mol.% ZrO_2), after electron beam irradiation, phosphorescence is observed with hyberbolic law of intensity decrease. The phosphorescence center is an unstable electron-hole pair which represents $Yb^{2+}{-}O^{1-}$.

These observed effects are assumed to be caused by distortion of crystalline polyhedra in the vicinity of the impurity zirconium ions.

Funding

This study was supported financially by the grant No. 24-19-20074 from the Russian Science Foundation https://rscf.ru/project/24-19-20074/, with the financial support of the Government of Sverdlovsk Region.

Conflict of interest

The authors declare that they have no conflict of interest.

References

[1] S.N. Bagayev, V.V. Osipov, V.A. Shitov, E.V. Pestryakov, V.S. Kijko, R.N. Maksimov, K.E. Lukyashin, A.N. Orlov, K.V. Polyakov, V.V. Petrov. J. Eur. Ceram. Soc. **32**, *16*, 4257 (2012).
[2] J. Lu, K. Takaichi, T. Uematsu, A. Shirakawa, M. Musha, K. Ueda, H. Yagi, T. Yanagitani, A.A. Kaminskii. Jpn. J. Appl. Phys. **41**, *12A,* L1373 (2002).
[3] K. Takaichi, H. Yagi, J. Lu, J.-F. Bisson, A. Shirakawa, K. Ueda, T. Yanagitani, A.A. Kaminskii. Appl. Phys. Lett. **84**, *3*, 317 (2004).
[4] V.I. Solomonov, V.V. Osipov, V.A. Shitov, R.N. Maksimov, A.V. Spirina, A.S. Makarova, A.N. Orlov, O.N. Tchaikovskaya, A.A. Shchukina, M.S. Snegerev, Yu.V. Kistenev. ZhPS **92**, *3*, 326 (2025). (in Russian).
[5] K.K. Bobkov, A.A. Rybaltovsky, V.V. Vel'miskin, M.E. Likhachev, M.M. Bubnov, E.M. Dianov, A.A. Umnikov, A.N. Gur'yanov, N.N. Vechkanov, I.A. Shestakova. Quantum Electron. **44**, *12*, 1129 (2014).
[6] V.V. Osipov, V.V. Platonov, V.V. Lisenkov, E.V. Tikhonov, A.V. Podkin. Appl. Phys. A **124**, *1*, 3 (2018).
[7] V.I. Solomonov, S.G. Michailov, A.I. Lipchak, V.V. Osipov, V.G. Shpak, S.A. Shunailov, M.I. Yalandin, M.R. Ulmaskulov. Laser Phys. **16**, *1*, 126 (2006).
[8] V.I. Solomonov, A.V. Spirina, S.F. Konev, S.O. Cholakh. Opt. Spectrosc. **116**, *5*, 793 (2014).
[9] D.V. Ananchenko, S.V. Nikiforov, G.R. Ramazanova, R.I. Batalov, R.M. Bayazitov, H.A. Novikov. Opt. Spectrosc. **128**, *2*, 207 (2020).
[10] G. Schaack, J.A. Koningstein. J. Opt. Soc. Am. **60**, *8*, 1110 (1970).
[11] M.V. Eremin. Opt. i spektr. **29**, *1*, 100 (1970). (in Russian).
[12] T.S. Piper, J.P. Brown, D.S. McClure. J. Chem. Phys. **46**, *4*, 1353 (1967).

Translated by M.Verenikina